sustainability

Article

An Intensity Measure for the Rocking Fragility Analysis of Rigid Blocks Subjected to Floor Motions

Hanquan Liu [1], Yong Huang [2,3] and Xiaohui Liu [1,*]

[1] Institute of Engineering Mechanics, China Earthquake Administration, No.1 Chaobai Street, Sanhe 065201, China
[2] Key Lab of Structural Dynamic Behavior and Control of the Ministry of Education, School of Civil Engineering, Harbin Institute of Technology, 73 Huanghe Road, Harbin 150090, China
[3] Key Lab of Smart Prevention and Mitigation of Civil Engineering Disasters of the Ministry of Industry and Information Technology, Harbin Institute of Technology, 73 Huanghe Road, Harbin 150090, China
* Correspondence: iemliuxh@163.com

Abstract: A novel intensity measure (*IM*), dimensionless floor displacement, is presented for evaluating the seismic fragility of freestanding rigid blocks subjected to one-sine acceleration pulses in this paper. The rocking responses of rigid blocks are simulated using an equivalent single-degree-of-freedom (SDOF) model with a bespoke discrete damper to account for energy dissipation. The performance of various *IM*s is compared using simulation results for four different block models under different excitation conditions. In comparison to some well-known *IM*s, the proposed *IM*, determined by excitation magnitude and frequency as well as block geometry parameters, displays a considerably stronger correlation with the peak rotation of the rocking block. The comparative results show that effective *IM*s should consider not only the excitation characteristics but also the block geometric parameters. Finally, the fragility curve generated by the proposed *IM* performs best by significantly reducing the dispersion.

Keywords: rigid blocks; rocking rotation; fragility curves; intensity measure; regression analysis; dispersion

check for updates

Citation: Liu, H.; Huang, Y.; Liu, X. An Intensity Measure for the Rocking Fragility Analysis of Rigid Blocks Subjected to Floor Motions. *Sustainability* **2023**, *15*, 2418. https://doi.org/10.3390/su15032418

Academic Editors: Yutao Pang, Xiaohui Yu, Junsheng Su and Xiyin Zhang

Received: 26 December 2022
Revised: 25 January 2023
Accepted: 27 January 2023
Published: 29 January 2023

1. Introduction

After an earthquake, it may be prohibitively costly to restore the functionality of a building with severe content damage [1], thus calling for the evaluation of building content damage [2]. An inhibition of evaluating the seismic damage of building contents is that predicting the response of such objects is extremely difficult. Unanchored contents in buildings, typically considered as freestanding rigid blocks, may undergo complex motions during earthquake events, including sliding, twisting, rocking, impacting neighboring walls or other objects, and even overturning due to floor movement. Within these complex dominating modes of motion, rocking and sliding are deemed to be of the most importance. Since Shenton [3] presented criteria for the initiation of the different response modes of an unanchored rigid block, the sliding response, among one of the dominating modes, has been addressed separately at great length [4–11]. This paper focuses on the freestanding rigid blocks dominated only by rocking motion, which features a partial uplift from its base and a change in rotation center, and overturning may occur when the rocking rotation is large enough.

As a very early study in this area, Housner [12] proposed a seminal framework to evaluate the seismic response of a solitary rigid block placed on a rigid base. Following this pioneering work, investigators over the world have endeavored to evaluate the rocking response of freestanding blocks, including experimental [13–24] and numerical approaches [25–39]. Early researchers have observed that a rocking motion has extremely complex dynamic characteristics and is barely “nonrepeatable” [40–43]. Even small changes in size, slenderness, or the details of ground motion might result in significant distinction in the rocking response. The reason for this phenomenon can be mainly attributed to the negative stiffness of rocking oscillators [44] and the complex variability in energy dissipation and transfer [45]. In this context, Yim [41] observed that systematic trends emerge when the rocking response is studied from a probabilistic point of view, with the excitation modeled as a random process [43]. Following the same idea, many investigators assessed the seismic performance of rigid blocks (e.g., rocking columns [46], bridges [47], and hospital contents [48]) via fragility analysis, a widely used method in earthquake engineering [49]. The rocking fragility is represented by a conditional probability that the damage measure (*DM*) will exceed a certain capacity limit state, given an *IM* value.

As the nonlinearity of the rocking oscillator is complex, widely used intensity measures proposed for elastic or elastoplastic oscillators are impracticable. Accordingly, many researchers have proposed various *IM*s for the fragility analysis of rocking blocks. Dimitrakopoulos and Paraskeva [50] explored different intensity measures in rocking and overturning fragility analysis. The results indicated that bivariate *IM*s provide superior estimations of the fragility to those adopting univariate ones, and dimensionless *IM*s are recommended for providing an approximate universal description of the rocking behavior. Petrone et al. [51] evaluated the efficiency of different *IM*s in predicting the probability that rigid blocks reach a specific damage state. In their research, dimensionless peak ground acceleration is demonstrated to be the most effective *IM* for small rigid blocks, whereas dimensionless peak ground velocity is the most effective one for large rigid blocks. Based on the dimensionless peak velocity, Sieber et al. [52] proposed a new *IM* considering the coefficient of restitution [12] of rigid blocks and obtained more universal results. However, the existing *IM*s present insufficiently strong correlations to the rocking response, thus causing large dispersion of the fragility curves.

To extend these studies, this paper presents a rigorous probabilistic investigation of the rocking response and assesses various *IM*s on their capability of describing the rocking response. The rocking responses of rigid blocks have been simulated with a reliable numerical model [53]. The motivation of this work is to propose a novel *IM* that considers not only the excitation characteristics but also the block geometric parameters, to gain a stronger correlation with the rocking response and less dispersion of the fragility curve. Consequently, the new *IM*, based on dimensionless floor displacement, is then proposed in this paper and evaluated through statistical analysis. The proposed *IM* exhibits a much stronger correlation with the dimensionless peak rotation of rocking blocks than the existing ones, thus greatly reducing the dispersion of the rocking fragility functions.

The rest of this paper is organized as follows. In Section 2, the rocking seismic response is simulated by adopting a discretely damped SDOF model, and the numerical model is validated using the experimental results. In Section 3, a three-dimensional rocking spectrum is derived as an extension of Zhang and Markris's overturning acceleration spectrum [54]. In Section 4, we propose a new intensity measure and demonstrate its superiority by comparing its performance in rocking fragility analysis with some widely used intensity measures. Finally, in Section 5, some concluding remarks are drawn. The definitions of symbols used in this paper are listed in Appendix A.

2. Rocking Seismic Response Analysis

2.1. Numerical Model of the Rocking Block

A homogenous freestanding rigid block with a width of $2b$ and a height of $2h$ is illustrated in Figure 1. The base surface is assumed to be horizontal, rigid, and rough enough so that rocking is the only dominating mode of motion. The total mass of the block is m, and the center of mass (CM) is also its center of geometric. Equivalently, the geometry of the block can be represented by a size parameter, $R = \sqrt{b^2 + h^2}$, which is the distance from CM to the pivot point, and a slenderness parameter, $\alpha = \text{atan}(b/h)$. Its moment of inertia about the pivot point O or O′ is $I_O = \frac{4}{3}mR^2$.

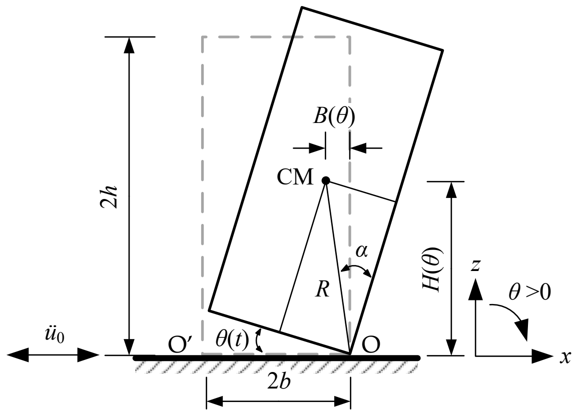

Figure 1. The geometry of a rocking block.

The rocking motion of the block can be fully described by the rotation θ around the pivot point. The moment equilibrium about the pivot point gives the equation of motion of an undamped rocking block under a horizontal excitation $\ddot{u}_0$:

$$I_O\ddot{\theta} - m\ddot{u}_0 H(\theta) + mgB(\theta) = 0 \tag{1}$$

where g is the gravity acceleration, $H(\theta)$ and $B(\theta)$ are the vertical and horizontal transient distances between CM and the current pivot point, respectively (Equations (2) and (3)):

$$H(\theta) = R \cdot \cos[\alpha \cdot \mathrm{sgn}(\theta) - \theta] \tag{2}$$

$$B(\theta) = R \cdot \sin[\alpha \cdot \mathrm{sgn}(\theta) - \theta] \tag{3}$$

where sgn() is the sign function.

The block will uplift and commence rocking when the horizontal excitation acceleration $\ddot{u}_0$ exceeds a minimum magnitude $g$tanα (Equation (4)). Once the rigid block starts to rock from the initial position, the restoring moment M decreases monotonically with the increase in the rotation θ, and reaches zero when θ = α, as shown by the light solid line in Figure 2. The M-θ relationship can be expressed in Equation (5). The maximum restoring moment at the initial position ($\theta = 0$) is denoted as M_0 (Equation (6)).

$$\ddot{u}_0 \geq gb/h = g \cdot \tan\alpha \tag{4}$$

$$M = mgR \cdot \sin[\alpha \cdot \mathrm{sgn}(\theta) - \theta] \tag{5}$$

$$M_0 = mgh \cdot \tan\alpha = mgR \cdot \sin\alpha \tag{6}$$

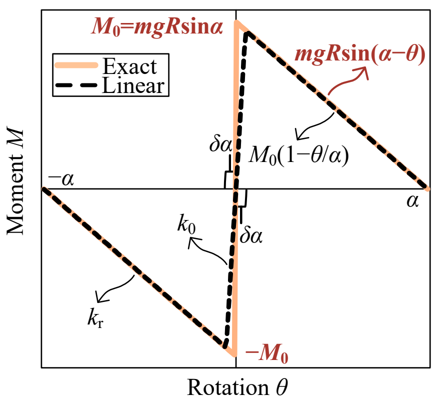

Figure 2. Moment–rotation relationship of a rocking block.

When the rocking block switches pivot corners and impacts the floor, there is some kinetic energy lost. The energy dissipation due to impact is commonly modeled by the restitution coefficient e, which is the ratio of the relative velocity of the rocking objects after and before the collision [55]. In this case, $e = \dot{\theta}_2/\dot{\theta}_1$, where $\dot{\theta}_1$ and $\dot{\theta}_2$ are the angular velocities before and after the block impacts with the floor. Housner [12] derived a rigid-body restitution coefficient e_R, represented by the slenderness parameter α of the block (Equation (7)), by conserving angular momentum before and immediately after the impact when the pivot point shifts from O to O′. The restitution coefficient e of a real-world collision also depends on the localized nonlinearity of the colliding materials and, therefore, is usually smaller than e_R [56].

$$e_R = \frac{I_O - 2mR^2 \sin^2 \alpha}{I_O} = 1 - \frac{3}{2} \sin^2 \alpha \tag{7}$$

In this paper, an equivalent lumped mass single-degree-of-freedom (SDOF) model is adopted to simulate the rocking response of freestanding blocks [57]. The lumped mass is modeled to be supported by a rigid link above the floor with a nonlinear elastic rotational spring at the base (Figure 3).

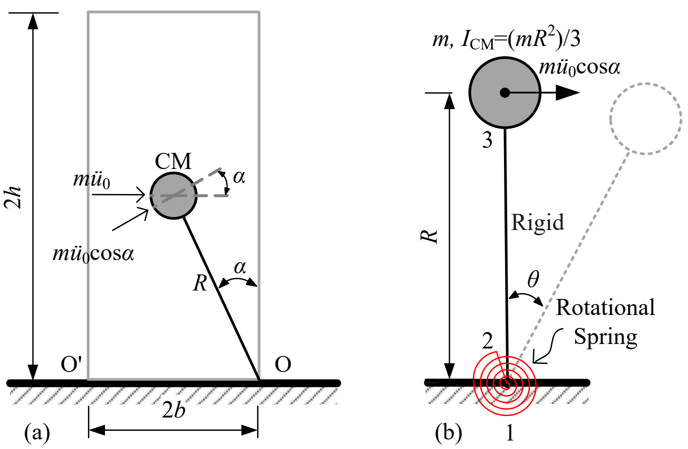

Figure 3. (**a**) Lumped mass representation of rigid block and (**b**) equivalent SDOF model of a rigid rocking block.

Considering a typical rocking block with geometry as illustrated in Figure 3a, the equation of motion of its equivalent SDOF oscillator (Figure 3b) subjected to a floor motion $\ddot{u}_0$ can be written as follows:

$$I_O\ddot{\theta} + f_d\left(\dot{\theta}\right) + k(\theta) \cdot \theta = -I_O\frac{\ddot{u}_0 \cos \alpha}{R} \tag{8}$$

where $I_O = \frac{4}{3}mR^2$ is the moment of inertia about the pivot point. f_d is the damping force to dissipate energy during rocking; k is the tangent stiffness to model the M-θ relationship of the rocking block. Since the moment of inertia of the lumped mass m is only mR^2, an additional moment of inertia $I_{CM} = \frac{mR^2}{3}$ is added in the model so that the total moment of inertia of the equivalent SDOF oscillator about the pivot point equals that of the original rigid block. The nonlinear M-θ relationship of the rocking block is embedded in the zero-length rotational spring at the bottom of the rigid link (Figure 3b). The nonlinear descending branch of the M-θ relationship is simplified to a linear relationship in Equation (9) (dashed line in Figure 2). Thus, the M-θ relationship embedded in the model is simplified as a bilinear elastic relationship with an initial stiffness k_0 within a small range, and a negative stiffness k_r beyond this range. $k_0 = n|k_r|$ is used to approximate the infinite stiffness before the rigid block starts to rock, where n is a large number. The system is assumed to oscillate linearly within the small range of $\pm\delta\alpha$ on both sides of the position $\theta = 0$, where $\delta = 1/(n+1)$.

$$M = mgR\sin\alpha \cdot \left(1 - \frac{\theta}{\alpha}\right) = M_0\left(1 - \frac{\theta}{\alpha}\right) \tag{9}$$

$$k(\theta) = \begin{cases} k_0 = n|k_r|, & |\theta|/\alpha \le \delta \\ k_r = -M_0/\alpha, & |\theta|/\alpha > \delta \end{cases} \tag{10}$$

A damping force $f_d\left(\dot{\theta}\right)$ is introduced to the simplified SDOF model to approximately account for the energy dissipation during rocking. Unlike the continuous damping model commonly used [44,58,59], a discrete damping model proposed by Liu et al. [53] is adopted to correctly simulate the energy dissipation. In this model, a viscous damping force $f_d = c_D\dot{\theta}$ applies only within the small range of $\pm\delta\alpha$ on both sides of the original position $\theta = 0$; when θ goes out of this range, the damping force equals 0; thus, the energy is dissipated if and only if the system passes its original position during rocking (Equation (11))

$$f_d\left(\theta, \dot{\theta}\right) = \begin{cases} c_D\dot{\theta}, & |\theta|/\alpha \le \delta \\ 0, & |\theta|/\alpha > \delta \end{cases} \tag{11}$$

where c_D is the discrete viscous damping coefficient. The coefficient c_D is not constant, but proportional to the angular velocity before each impact (Figure 4), which is physically associated with the restitution coefficient during impact by the conservation of angular momentum $\dot{\theta}_1$ (Equation (12)). The restitution coefficient $e = 0.95e_R$ is adopted to consider the energy dissipation of a real-world collision. The numerical simulation is performed in OpenSees [60], and the technical details can be found in our former paper [53].

$$c_D = \frac{I_O}{2\delta\alpha}(1 - e)\left|\dot{\theta}_1\right| \tag{12}$$

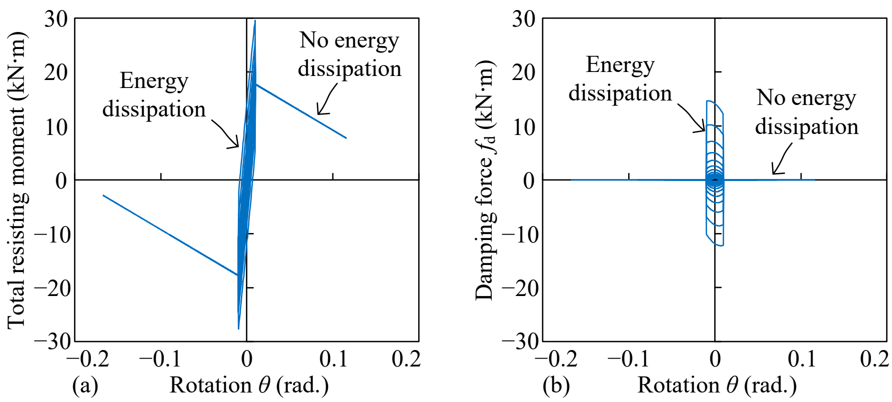

Figure 4. Hysteretic curves of a free-rocking SDOF system of $\alpha = 0.2$ and $R = 0.38$ m: (**a**) total resisting moment with discrete damping, (**b**) discrete damping force.

2.2. Experimental Verifications

To demonstrate the superior performance of the discrete damping model, the simulated results are compared with the experimental results from Nasi [61–63] (Figure 5). Six selected runs of simulated response histories are compared with experimental results in Figure 6. The accuracy and the applicability of this model have been demonstrated by correctly approximating the maximum rotation angle and successfully estimating the occurrence of overturning [53].

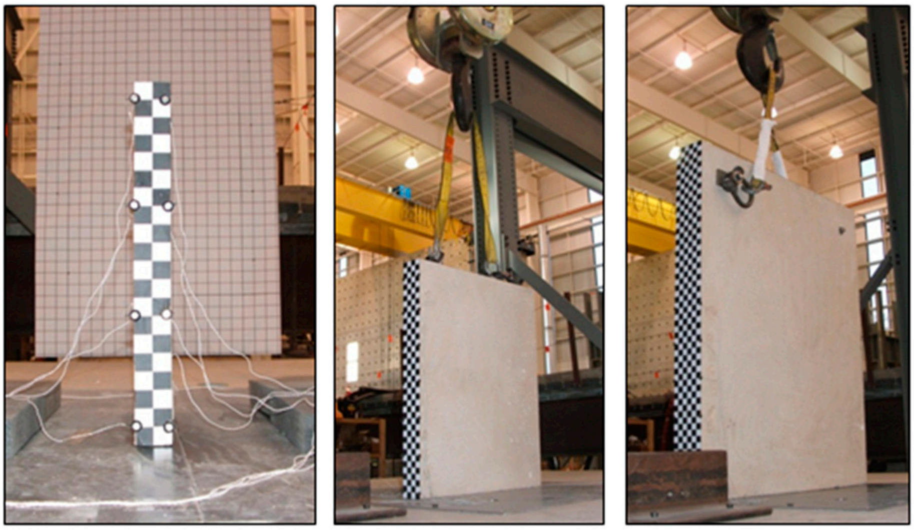

Figure 5. Experimental set up (source: PURR—Stability_of_Rocking_Structures_20170825 (purdue.edu), accessed on 24 December 2022).

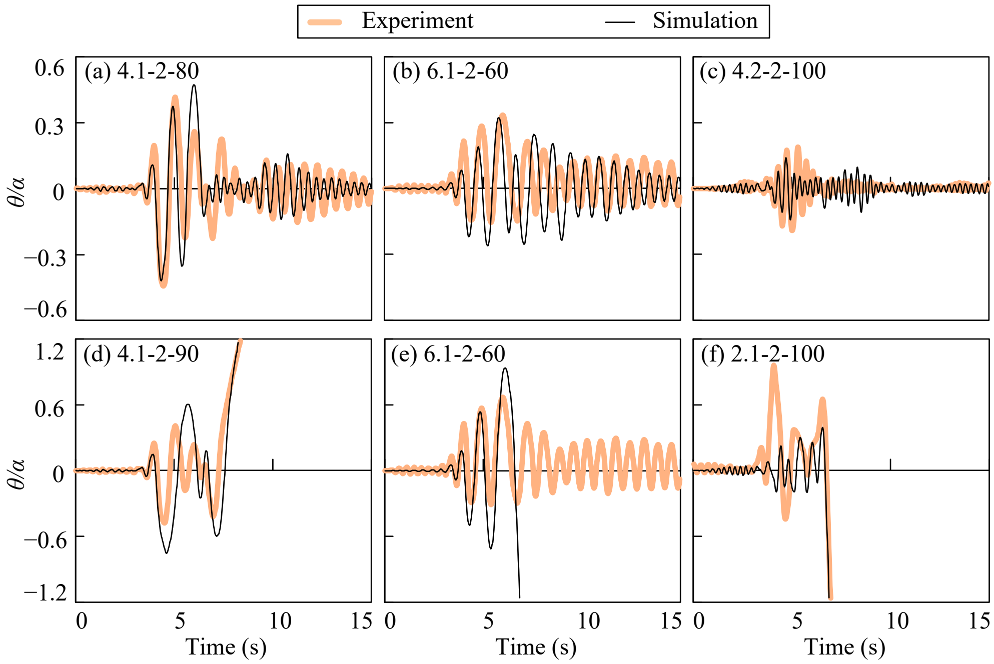

Figure 6. Comparison of rotation histories of non-overturning (**a**–**c**) and overturned (**d**–**f**) runs by SDOF models.

3. Rocking Spectra

Zhang and Makris [54] proposed an overturning acceleration spectrum for freestanding rigid blocks subjected to one-sine acceleration pulses. The two axes of the spectrum are dimensionless pulse frequency (ω_P/P) and dimensionless peak pulse acceleration ($PFA/g\tan\alpha$), where T_p and $\omega_P = 2\pi/T_P$ are the period and circular frequency of the pulse excitation, respectively. PFA is peak floor acceleration, and $P = \sqrt{3g/4R}$ is the frequency parameter of the rigid block proposed by Housner [12]. Although the coordinate plane in the literature [54] is divided into three zones of overturning, without impact, overturning with impact, and no overturning, to focus on overturning probability, the overturning acceleration spectrum in this study is divided simply into the overturning zone and safe zone.

The overturning acceleration spectrum is evaluated by simulating the overturning responses of the four rigid block models (Figure 7) by the simplified SDOF model with discrete damping. The geometry parameters of the four models are listed in Table 1, which are common sizes of objects around us. With each model excited by 100 pulses, 400 uniformly distributed cases are obtained in an overturning acceleration spectrum by adjusting the *PFA* and ω_P of one-sine pulse motions (Figure 8a). There is a clear boundary between the overturning zone and the safe zone in the overturning acceleration spectrum obtained from one-sine pulse motions (Figure 8b), which is also in line with the results of Zhang and Makris [54].

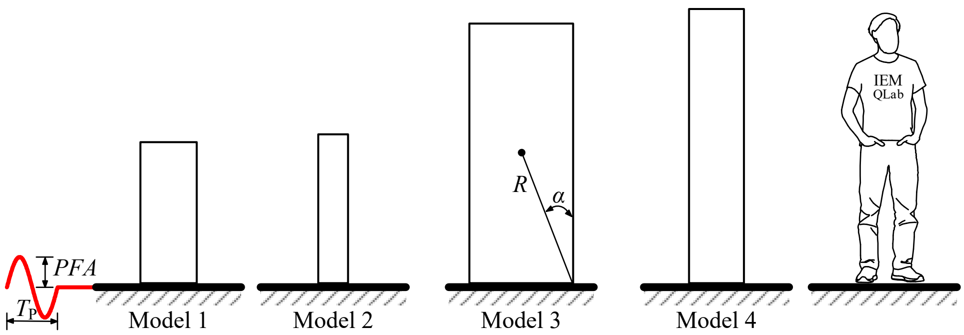

Figure 7. Schematic illustration of the investigated rocking block geometries.

Table 1. Geometry parameters of rigid block models.

	$2b$ (m)	$2h$ (m)	R (m)	α	P
Model 1	0.3785	0.9462	0.5095	0.3805	3.7981
Model 2	0.1999	0.9993	0.5095	0.1974	3.7981
Model 3	0.6971	1.7427	0.9385	0.3805	2.7986
Model 4	0.3681	1.8405	0.9385	0.1974	2.7986

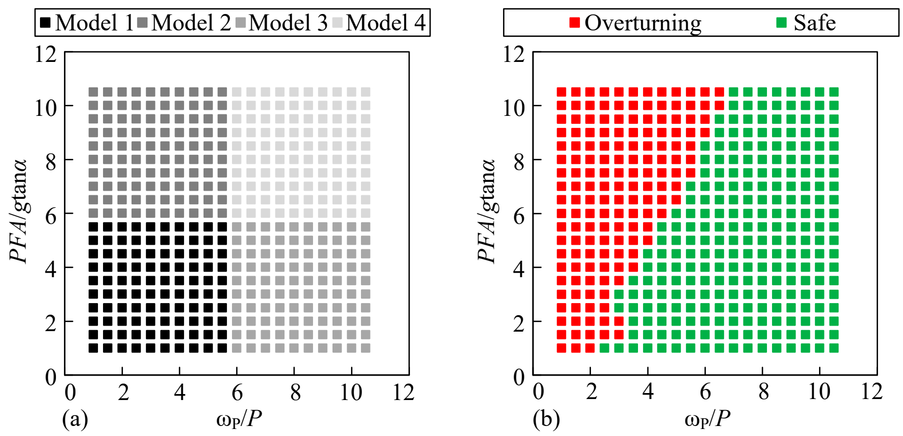

Figure 8. (**a**) Model distribution and (**b**) seismic responses of blocks subjected to one-sine pulse.

Three-dimensional rocking rotation spectrum can be obtained by extending the overturning acceleration spectrum with the third axe being the normalized peak rocking rotation $|\theta_{\max}|/\alpha$, as shown in Figure 9. It can be observed that the peak rocking rotation is not only related to ω_P/P but also $PFA/g\tan\alpha$, which are usually used as intensity measures. However, it is obvious that either one is one-sided for rocking fragility analysis, which leads to the superiority of bivariate *IMs* [50]. An *IM*, for rocking fragility analysis, should be defined not only by the excitation characteristics (magnitude *PFA*, frequency ω_P) but also by the geometric parameters of the rigid block (size parameter R, slenderness parameter α).

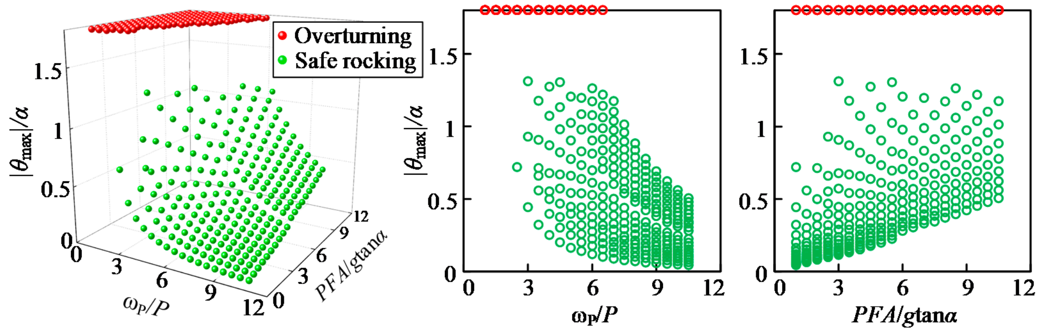

Figure 9. Three-dimensional rocking rotation spectrum.

4. Rocking Fragility Analysis

The rocking fragility of the freestanding rigid blocks can be expressed as the conditional probability P_f that a damage measure (*DM*) will exceed a certain capacity limit state (*LS*), given an *IM* value:

$$P_f = P(DM > LS|IM) \tag{13}$$

The probability tree diagram that incorporates the peculiarities of the rocking response and facilitates the calculation of conditional probability P_f is depicted in Figure 10. P_{nr} denotes the probability that the rigid block will remain resting on the ground (non-rocking response) throughout the excitation. This case corresponds to the fact that the block does not rock unless the acceleration $\ddot{u}_0$ exceeds the minimum threshold in Equation (5). P_{ro} denotes the rocking–overturning probability. The probability P_f that the *DM* will exceed a certain capacity limit *LS* given an *IM* value is derived by the union of two likelihoods (Figure 10), namely, the probability P_{ro} of overturning caused by rocking and the probability P_{ex} that the *DM* will exceed the threshold *LS* during rocking response without the occurrence of overturning. This paper focuses on the calculation and analysis of the latter, i.e., the probability P_{ex} that the *DM* will exceed the threshold *LS* during rocking response without overturning (safe rocking), and the performance of different *IM*s have been compared in this analysis process.

$$P_f = P_{ro} + (1 - P_{ro})P_{ex}(DM > LS|IM) \tag{14}$$

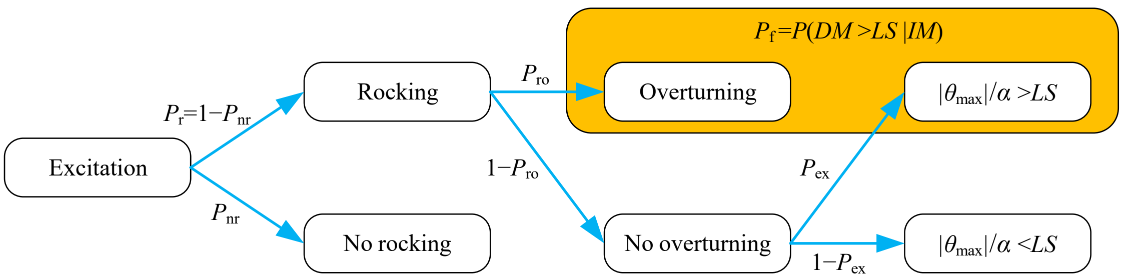

Figure 10. Probability tree diagram for the rocking problem.

4.1. Damage Measure and Limit States

Dimensionless *DM* has been widely used because it is straightforward to evaluate the degree of rocking response [50–52]. For the purposes of the subsequent fragility analysis, the absolute peak rocking rotation $|\theta_{max}|$ normalized by the slenderness angle α is used as the *DM* in this paper (Equation (16)). This dimensionless *DM* highlights its clear physical meaning: a larger-than-0 value corresponds to the rigid block commencing rocking, whereas higher values indicate that the block experiences more severe rocking. Three apposite performance levels are proposed to assess the vulnerability of a rocking block: LS_1 = 0.1 marks observable rocking during seismic excitation, LS_2 = 0.5 indicates moderate rocking response, and LS_3 = 1.0 corresponds to extremely severe rocking. The dimensionless absolute peak rocking rotation $|\theta_{max}|/\alpha$ is regularly used to judge whether the blocks are overturned or not, with greater-than-1.0 values denoting overturning [52,64]. However, this viewpoint is deemed to be controversial because a few studies have also pointed out that it is still possible for $|\theta_{max}|$ to exceed α without overturning [54]. Moreover, the fragility analysis results obtained by the data of safe rocking are based on the premise that no overturning occurs. That is to say, a high value of the *DM* (even *DM* >1.0) merely means that the rigid block may rock violently, and it is very likely to return to its original configuration eventually.

$$DM = \frac{|\theta_{max}|}{\alpha} \tag{15}$$

4.2. Intensity Measures

As stated above, discovering appropriate *IM*s for rocking fragility analysis has been a pending challenge for a long time. A summary and examination of eight commonly used dimensionless *IM*s are presented in this paper, along with a comparison with the proposed *IM*. IM_1, IM_2, and IM_3 are dimensionless floor motion frequency, dimensionless peak floor acceleration, and dimensionless peak floor velocity, respectively:

$$IM_1 = \frac{\omega_P}{P},\ \ IM_2 = \frac{PFA}{g\tan\alpha},\ \ IM_3 = \frac{P\cdot PFV}{g\tan\alpha} \tag{16}$$

where *PFV* is the peak velocity of the pulse and $P = \sqrt{3g/4R}$ is the frequency parameter [12]. Then, IM_4, IM_5, IM_6, and IM_7 are the four bivariate *IM*s proposed by Dimitrakopoulos and Paraskeva [50], of which the first two are often used for rocking fragility analysis and the last two for overturning fragility analysis:

$$IM_4 = 1.484\left(\frac{PFA}{g\tan\alpha}\right)^{1.644}\left(\frac{\omega_P}{P}\right)^{-2.013} \tag{17}$$

$$IM_5 = 0.063\left(\frac{PFA}{g\tan\alpha}\right)^{2.954}\left(\frac{\omega_P}{P}\right)^{-0.942} \tag{18}$$

$$IM_6 = \left(\frac{PFA}{g\tan\alpha}\right)^{0.52}\left(\frac{\omega_P}{P}\right)^{-0.48} \tag{19}$$

$$IM_7 = \left(\frac{PFA}{g\tan\alpha}\right)^{0.6}\left(\frac{\omega_P}{P}\right)^{-0.4} \tag{20}$$

IM_8 is a newly proposed *IM* based on the dimensionless peak velocity that takes into account the restitution coefficient e_R (Equation (7)). This *IM* has been tested extensively and has been shown to produce universal results in the literature [52].

$$IM_8 = \frac{{e_R}^4\cdot P\cdot PFV}{g\tan\alpha} \tag{21}$$

Following the same idea of dimensionless *IM*, we propose a new *IM* (i.e., IM_9) in this study. IM_9 explicitly includes excitation characteristics (magnitude *PFA* and frequency ω_P) and geometric parameters of the rigid block (size parameter *R* and slenderness parameter α). The proposed IM_9, which can be regarded as a dimensionless displacement intensity measure, has been compared with the eight *IM*s mentioned above in the subsequent rocking fragility analysis.

$$IM_9 = \frac{PFA\cdot {T_P}^2}{R\tan\alpha} \tag{22}$$

4.3. Probability of Limit State Exceedance during Safe Rocking

Assuming that the *DM* and *IM* are random variables following lognormal distributions, the conditional probability P_{ex} that an excitation with *IM* = x will cause the damage exceedance of a capacity limit *LS* during safe rocking can be written as follows:

$$P_{ex} = P_{ex}(DM > LS|IM = x) = 1 - \Phi\left(\frac{\ln(LS) - \mu(x)}{\beta}\right) \tag{23}$$

where Φ is the standard (i.e., with mean 0 and standard deviation 1) normal cumulative distribution function, μ is the median value of natural logarithm of x (ln$x$), and β is the dispersion, or logarithmic standard deviation.

Assume there is a linear relationship between μ and ln(*IM*)

$$\mu = a + b\ln(IM) \tag{24}$$

which is a typical trick that facilitates the estimation of parameters a and b through linear regression analysis (Figure 11). Additionally, the dispersion β can be obtained by Equation (25). According to Equation (23), given a capacity limit *LS*, the corresponding fragility curves of the freestanding rigid blocks during safe rocking can be obtained. A lower value of β means less dispersion of the demand and, consequently, a more efficient *IM*.

$$\beta = \sqrt{\frac{1}{n-1}\sum_{i=1}^{n}(\ln DM_i - \mu(x_i))^2} \tag{25}$$

Figure 11 presents the linear regression results of the *DM* with respect to different *IMs* in logarithmic space, considering only the cases of safe rocking. The fitting parameters a, b, and dispersion β are shown in Table 2. The coefficient of determination R^2, which is used to evaluate the efficiency of the regression, is also included. A closer-to-1 R^2 value indicated better goodness of fit. Among the commonly used univariate *IM*s, dimensionless peak floor velocity IM_3 performs the best, with a smaller β and larger R^2. This is consistent with previous research results [22,51,64]. Compared with univariate *IM*s, the four bivariate *IM*s proposed by Dimitrakopoulos and Paraskeva [50] generally produce better results overall, with IM_4 performing particularly well. The new IM_9 proposed in this paper exhibits a much stronger correlation with the *DM* in logarithmic space than all the existing *IM*s examined in this paper, with the smallest β and the largest R^2. Therefore, we recommend using IM_9 as an intensity measure for rocking fragility analysis.

Table 2. Linear regression analysis parameters of different *IM*s.

IM	*a*	*b*	β	R^2
IM_1	1.1730	−1.0999	0.7083	0.1846
IM_2	−2.1786	0.8195	0.5597	0.4908
IM_3	−0.3761	1.1643	0.2569	0.8928
IM_4	−0.1313	0.7151	0.1827	0.9457
IM_5	−0.8771	0.3274	0.4765	0.6310
IM_6	−0.5569	2.2191	0.2829	0.8699
IM_7	−1.1339	1.8261	0.3689	0.7788
IM_8	−0.0879	0.7671	0.3782	0.7675
IM_9	−2.5232	1.0484	0.1113	0.9799

The rocking fragility curves obtained by various *IM*s according to the three performance thresholds mentioned above are shown in Figure 12. The proposed IM_9, with the smallest dispersion β, consistently shows the steepest curve. The best-performing fragility curves have been obtained with respect to the most effective IM_9, which can conveniently estimate the probability P_{ex} that an excitation will cause the exceedance of a performance limit during safe rocking.

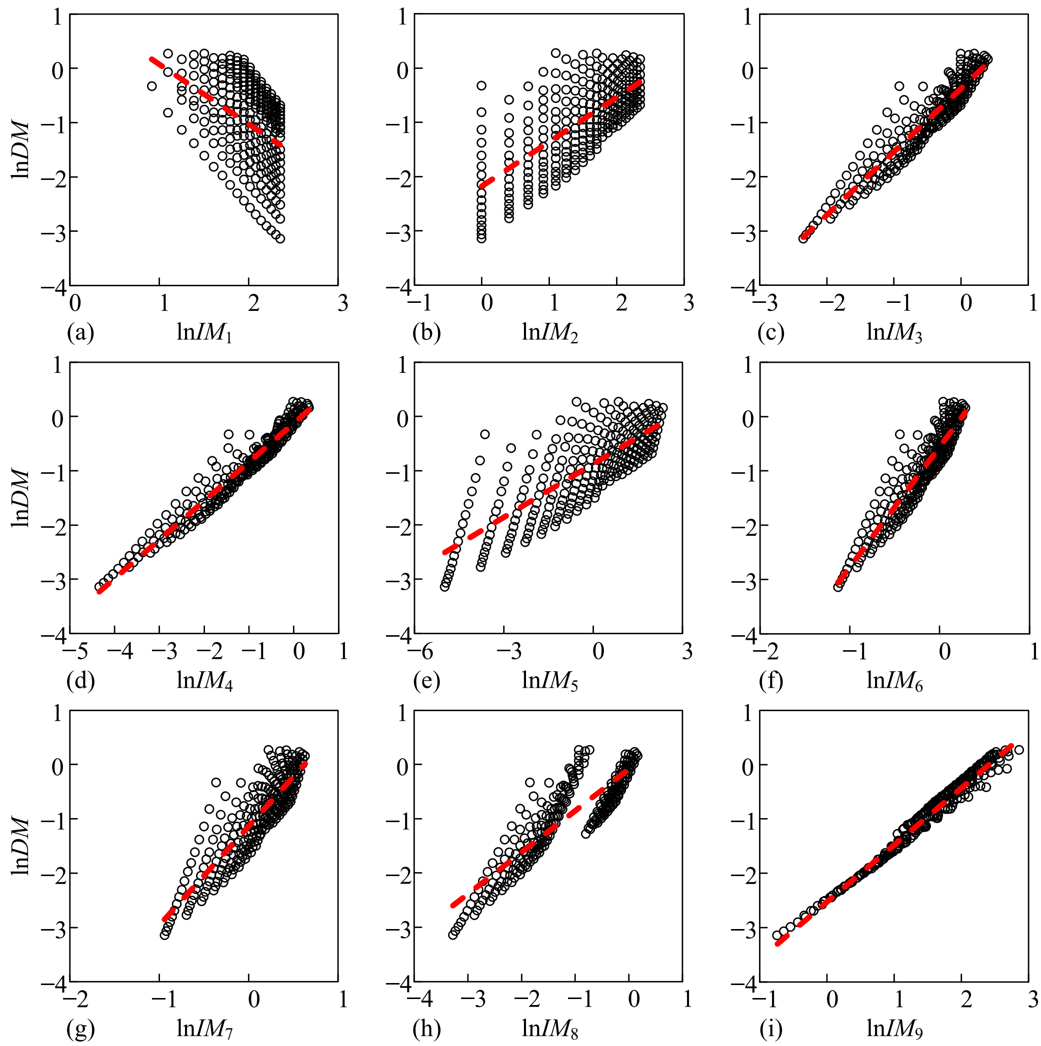

Figure 11. Linear regression analysis of the maximum normalized response with respect to different *IM*s: (**a**–**h**) IM_1–IM_8; (**i**) the proposed IM_9.

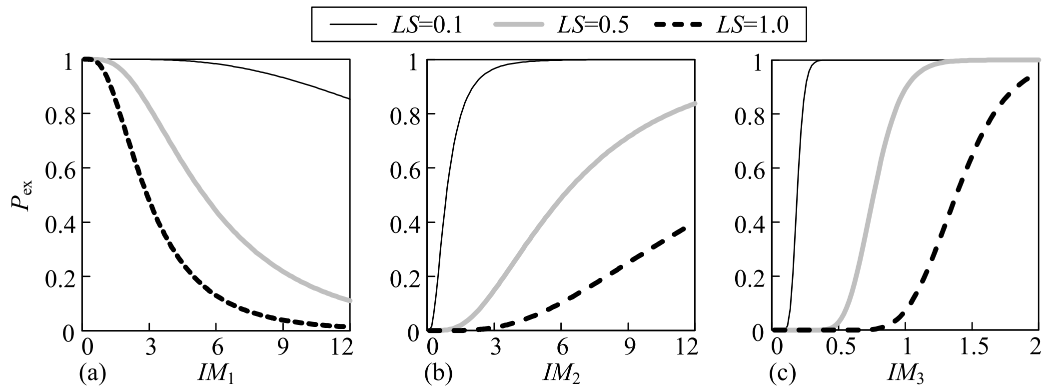

Figure 12. *Cont.*

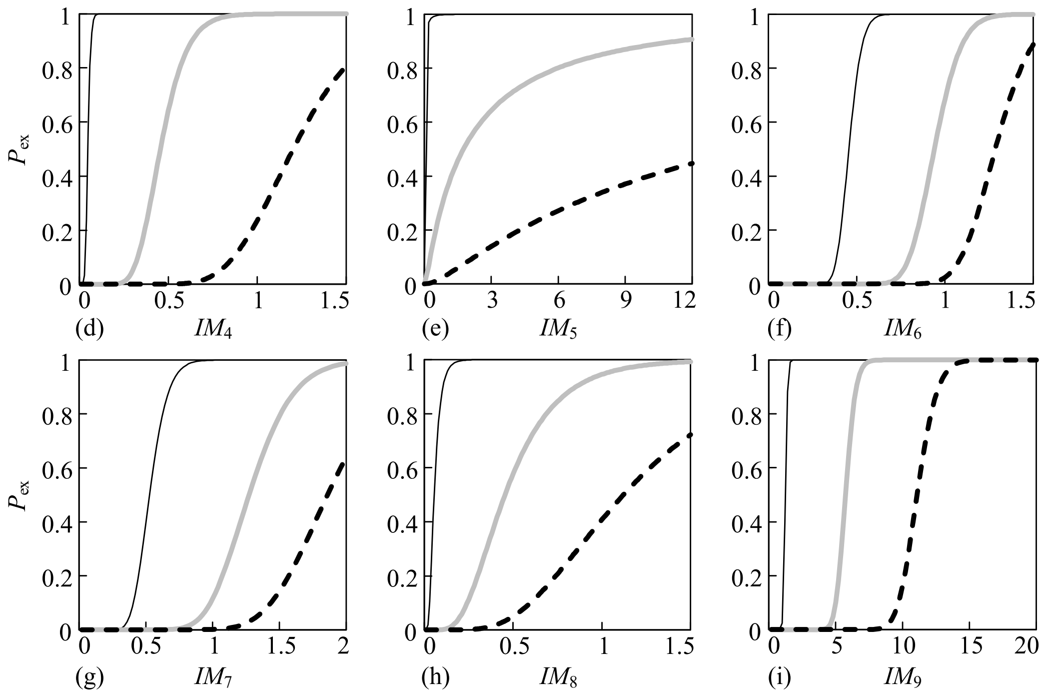

Figure 12. Rocking fragility curves for different *IM*s: (**a**–**h**) IM_1–IM_8; (**i**) the proposed IM_9.

5. Conclusions

This study examined the seismic behaviors of the freestanding rigid blocks subjected to one-sine acceleration pulses. We simulated four blocks, in common sizes of objects around us, under excitation with different amplitudes and different frequencies using a reliable numerical model. The seismic rocking fragility has been assessed within a probabilistic framework. Eight well-established intensity measures, along with a new intensity measure proposed in this paper, were evaluated on their capability to describe the excitation-induced peak rocking rotation. With the cases of safe rocking solely studied here, the fragility curves were derived and approximated by fitting lognormal cumulative distributions. The following conclusions can be drawn from the results:

1. An effective *IM* should take into account not only the excitation characteristics (magnitude *PFA*, frequency ω_P) but also the geometric parameters of the rigid blocks (size parameter R, slenderness parameter α);
2. The dimensionless peak floor velocity performs better among the univariate *IM*s commonly used in rocking fragility analysis. Bivariate *IM*s perform better overall, but require more computation;
3. A novel *IM* explicitly including excitation characteristics and geometric parameters of the rigid blocks is proposed in this paper. The proposed *IM* exhibits a much stronger correlation with the *DM* in logarithmic space; consequently, the proposed *IM* yields the smallest β in linear regression analysis, which results in the best-performing fragility curves;
4. Future studies should aim at evaluating the overturning fragility, as well as the rocking behavior subject to excitations in the real world.

Author Contributions: Conceptualization, H.L. and X.L.; methodology, H.L. and X.L.; software, H.L. and X.L.; validation, H.L. and X.L.; investigation, H.L., Y.H. and X.L.; writing—original draft preparation, H.L., Y.H. and X.L.; writing—review and editing, H.L., Y.H. and X.L. All authors have read and agreed to the published version of the manuscript.

Funding: This research received no external funding.

Institutional Review Board Statement: Not applicable.

Informed Consent Statement: Not applicable.

Data Availability Statement: Not applicable.

Acknowledgments: We thank Lucas Laughery for generously sharing the experimental data in their data paper published in 2018.

Conflicts of Interest: The authors declare no conflict of interest.

Appendix A

Table A1. Definition of symbols used in this paper.

Symbol	Definition
$2b$	Width
$2h$	Height
R	Size parameter
α	Slenderness parameter
I_O	Moment of inertia
θ and $\ddot{\theta}$	Rotation angle and rotational angular acceleration
$\ddot{u}_0$	Horizontal excitation
H and B	Vertical and horizontal transient distances
g	Gravity acceleration
M	Restoring moment
M_0	Maximum restoring moment
$\dot{\theta}_1$ and $\dot{\theta}_2$	Angular velocities before and after impacts
e	Restitution coefficient
e_R	Rigid-body restitution coefficient
f_d	Damping force
k	Tangent stiffness
I_{CM}	Additional moment of inertia
k_0	Initial stiffness
k_r	Negative stiffness
n	A large number
$\delta\alpha$	Small range around initial position
c_D	Discrete viscous damping coefficient
$\theta_{\max}$	Peak rocking rotation
T_p	Period of pulse excitation
ω_P	Circular frequency of pulse excitation
P	Block frequency parameter
PFA	Peak floor acceleration
PFV	Peak floor velocity
IM	Intensity measure
DM	Damage measure
LS	Limit state
P_f	Conditional probability
P_{ro}	Overturning probability
P_{ex}	Probability for DM exceeding LS within safe rocking
x	IM value
μ	Median value of $\ln x$
a and b	Linear regression parameters
β	Dispersion
R^2	Coefficient of determination

References

1. Taghavi, S.; Miranda, M.M. *Response Assessment of Nonstructural Building Elements*; Pacific Earthquake Engineering Research Center; University of California: Berkeley, CA, USA, 2003.
2. Majdalaweyh, S.; Pang, W. Empirical seismic fragility assessment and optimal risk mitigation of building contents. *Eng. Struct.* **2022**, *259*, 114183. [CrossRef]

3. Shenton, H.W., III. Criteria for initiation of slide, rock, and slide-rock rigid-body modes. *J. Eng. Mech.* **1996**, *122*, 690–693. [CrossRef]
4. Newmark, N.M. Effects of earthquakes on dams and embankments. *Géotechnique* **1965**, *15*, 139–160. [CrossRef]
5. Lopez Garcia, D.; Soong, T.T. Sliding fragility of block-type nonstructural components. Part 1: Freestanding components. *Earthq. Eng. Struct. Dyn.* **2003**, *32*, 111–129. [CrossRef]
6. Chaudhuri, S.R.; Hutchinson, T.C. Characterizing frictional behavior for use in predicting the seismic response of unattached equipment. *Soil Dyn. Earthq. Eng.* **2005**, *25*, 591–604. [CrossRef]
7. Konstantinidis, D.; Makris, N. Experimental and analytical studies on the response of freestanding laboratory equipment to earthquake shake. *Earthq. Eng. Struct. Dyn.* **2009**, *38*, 827–848. [CrossRef]
8. Gazetas, G.; Garini, E.; Berrill, J.B.; Apostolou, M. Sliding and overturning potential of Christchurch 2011 earthquake records. *Earthq. Eng. Struct. Dyn.* **2012**, *41*, 1921–1944. [CrossRef]
9. Nagao, T.; Kagano, H.; Hamaguchi, K. Full-Scale Shake Table Test on Furnitures Subjected to Long-Period Earthquake Motions. In Proceedings of the 15th World Conference on Earthquake Engineering, Lisbon, Portugal, 24–28 September 2012.
10. Konstantinidis, D.; Nikfar, F. Seismic response of sliding equipment and contents in base-isolated buildings subjected to broadband ground motions. *Earthq. Eng. Struct. Dyn.* **2015**, *44*, 865–887. [CrossRef]
11. Nikfar, F.; Konstantinidis, D. Peak sliding demands on unanchored equipment and contents in base-isolated buildings under pulse exitation. *J. Struct. Eng.* **2017**, *143*, 04017086. [CrossRef]
12. Housner, G.W. The behavior of inverted pendulum structures during earthquakes. *Bull. Seismol. Soc. Am.* **1963**, *53*, 403–417. [CrossRef]
13. Filiatrault, A.; Kuan, S.; Tremblay, R. Shake table testing of bookcase–partition wall systems. *Can. J. Civ. Eng.* **2004**, *31*, 664–676. [CrossRef]
14. Arredondo, C.; Jaimes, M.A.; Reinoso, E. A simplified model to evaluate the dynamic rocking behavior of irregular free-standing rigid bodies calibrated with experimental shaking-table tests. *J. Earthq. Eng.* **2019**, *23*, 46–71. [CrossRef]
15. Berto, L.; Meroi, E.; Rocca, I.; Saetta, A. Rocking activation of free standing elements in real conditions: A safe experimentally-based acceleration limit. *Eng. Struct.* **2021**, *226*, 111331. [CrossRef]
16. Peña, F.; Prieto, F.; Lourenço, P.B.; Costa, A.C.; Lemos, J.V. On the dynamics of rocking motion of single rigid-block structures. *Earthq. Eng. Struct. Dyn.* **2007**, *36*, 2383–2399. [CrossRef]
17. Kuo, K.C.; Suzuki, Y.; Katsuragi, S.; Yao, G.C. Shake table tests on clutter levels of typical medicine shelves and contents subjected to earthquakes. *Earthq. Eng. Struct. Dyn.* **2011**, *40*, 1367–1386. [CrossRef]
18. Konstantinidis, D.; Makris, N. Experimental and analytical studies on the response of 1/4-scale models of freestanding laboratory equipment subjected to strong earthquake shake. *Bull. Earthq. Eng.* **2010**, *8*, 1457–1477. [CrossRef]
19. Bachmann, J.A.; Blöchlinger, P.; Wellauer, M.; Vassiliou, M.F.; Stojadinovic, B. Experimental investigation of the seismic response of a column rocking and rolling on a concave base. In Proceedings of the ECCOMAS Congress, VII European Congress on Computational Methods in Applied Sciences and Engineering, Crete Island, Greece, 5–10 June 2016; pp. 5023–5062.
20. Huang, B.; Pan, Q.; Lu, W.; Shen, F. Free-rocking tests of a freestanding object with variation of center of gravity. *Earthq. Eng. Struct. Dynamics.* **2021**, *50*, 3015–3040. [CrossRef]
21. Vassiliou, M.F.; Broccardo, M.; Cengiz, C.; Dietz, M.; Dihoru, L.; Gunay, S.; Stojadinovic, B. Shake table testing of a rocking podium: Results of a blind prediction contest. *Earthq. Eng. Struct. Dyn.* **2021**, *50*, 1043–1062. [CrossRef]
22. Di Sarno, L.; Magliulo, G.; D'Angela, D. Experimental assessment of the seismic performance of hospital cabinets using shake table testing. *Earthq. Eng. Struct. Dyn.* **2019**, *48*, 103–123. [CrossRef]
23. Vassiliou, M.F.; Cengiz, C.; Dietz, M.; Dihoru, L.; Broccardo, M.; Mylonakis, G.; Stojadinovic, B. Data set from shake table tests of free-standing rocking bodies. *Earthq. Spectra* **2021**, *37*, 2971–2987. [CrossRef]
24. Liu, P.; Xue, W.; Pang, H.; Zhang, Y.M.; Chen, H.T.; Yang, W.G. Seismic overturning fragility analysis for freestanding building contents subjected to horizontal bidirectional floor motions. *Soil Dyn. Earthq. Eng.* **2022**, *161*, 107414. [CrossRef]
25. Ishiyama, Y. Motions of rigid bodies and criteria for overturning by earthquake excitations. *Earthq. Eng. Struct. Dyn.* **1982**, *10*, 635–650. [CrossRef]
26. Thiers-Moggia, R.; Málaga-Chuquitaype, C. Dynamic response of post-tensioned rocking structures with inerters. *Int. J. Mech. Sci.* **2020**, *187*, 105927. [CrossRef]
27. Chae, Y.B.; Kim, J.K. Implementation of configuration dependent stiffness proportional damping for the dynamics of rigid multi-block systems. *Earthq. Eng. Eng. Vib.* **2003**, *2*, 87–97. [CrossRef]
28. Di Egidio, A.; Zulli, D.; Contento, A. Comparison between the seismic response of 2D and 3D models of rigid blocks. *Earthq. Eng. Eng. Vib.* **2014**, *13*, 151–162. [CrossRef]
29. Vetr, M.G.; Nouri, A.R.; Kalantari, A. Seismic evaluation of rocking structures through performance assessment and fragility analysis. *Earthq. Eng. Eng. Vib.* **2016**, *15*, 115–127. [CrossRef]
30. Fragiadakis, M.; Kolokytha, M. Diamantopoulos, S. Seismic risk assessment of rocking building contents of multistorey buildings. *Procedia Eng.* **2017**, *199*, 3534–3539. [CrossRef]

31. Gesualdo, A.; Iannuzzo, A.; Minutolo, V.; Monaco, M. Rocking of freestanding objects: Theoretical and experimental comparisons. *J. Theor. Appl. Mech.* **2018**, *56*, 977–991. [CrossRef]
32. Kasinos, S.; Lombardo, M.; Makris, N.; Palmeri, A. Dynamic response analysis of nonlinear secondary oscillators to idealised seismic pulses. *Earthq. Eng. Struct. Dyn.* **2020**, *49*, 1473–1495. [CrossRef]
33. Reggiani Manzo, N.; Vassiliou, M.F. Simplified analysis of bilinear elastic systems exhibiting negative stiffness behavior. *Earthq. Eng. Struct. Dyn.* **2021**, *50*, 580–600. [CrossRef]
34. D'Angela, D.; Magliulo, G.; Cosenza, E. Towards a reliable seismic assessment of rocking components. *Eng. Struct.* **2021**, *230*, 111673. [CrossRef]
35. Aghagholizadeh, M. A finite element model for seismic response analysis of vertically-damped rocking-columns. *Eng. Struct.* **2020**, *219*, 110894. [CrossRef]
36. Vanin, F.; Penna, A.; Beyer, K. A three-dimensional macroelement for modelling the in-plane and out-of-plane response of masonry walls. *Earthq. Eng. Struct. Dyn.* **2020**, *49*, 1365–1387. [CrossRef]
37. Galvez, F.; Sorrentino, L.; Dizhur, D.; Ingham, J.M. Seismic rocking simulation of unreinforced masonry parapets and façades using the discrete element method. *Earthq. Eng. Struct. Dyn.* **2022**, *51*, 1840–1856. [CrossRef]
38. Scattarreggia, N.; Malomo, D.; DeJong, M.J. A new Distinct Element meso-model for simulating the rocking-dominated seismic response of RC columns. *Earthq. Eng. Struct. Dyn.* **2022**, 1–11. [CrossRef]
39. Vlachakis, G.; Giouvanidis, A.I.; Mehrotra, A.; Lourenço, P.B. Numerical block-based simulation of rocking structures using a novel universal viscous damping model. *J. Eng. Mech.* **2021**, *147*, 04021089. [CrossRef]
40. Aslam, M.; Godden, W.G.; Scalise, D.T. Earthquake rocking response of rigid bodies. *ASCE J. Struct. Div.* **1980**, *106*, 377–392. [CrossRef]
41. Yim, C.; Chopra, A.K.; Penzien, J. Rocking response of rigid blocks to earthquakes. *Earthq. Eng. Struct. Dyn.* **1980**, *8*, 565–587. [CrossRef]
42. Ibarra, L. *Seismic Performance of Dry Casks Storage for Long-term Exposure. Final Report*; University of Utah: Salt Lake City, UT, USA, 2016.
43. Bachmann, J.A.; Strand, M.; Vassiliou, M.F.; Broccardo, M.; Stojadinović, B. Is rocking motion predictable? *Earthq. Eng. Struct. Dyn.* **2018**, *47*, 535–552. [CrossRef]
44. Giannini, R.; Masiani, R. Risposta in frequenza del blocco rigido: Stabilita delle soluzioni. In Proceedings of the 10th Conference of the Italian Association of Theoretical and Applied Mechanics, Pisa, Italy, 2–6 July 1990.
45. Acikgoz, S.; Ma, Q.; Palermo, A.; DeJong, M.J. Experimental identification of the dynamic characteristics of a flexible rocking structure. *J. Earthq. Eng.* **2016**, *20*, 1199–1221. [CrossRef]
46. Roh, H.; Cimellaro, G.P. Seismic fragility evaluation of RC frame structures retrofitted with controlled concrete rocking column and damping technique. *J. Earthq. Eng.* **2011**, *15*, 1069–1082. [CrossRef]
47. Deng, L.; Kutter, B.L.; Kunnath, S.K. Probabilistic seismic performance of rocking-foundation and hinging-column bridges. *Earthq. Spectra* **2012**, *28*, 1423–1446. [CrossRef]
48. Cosenza, E.; Di Sarno, L.; Maddaloni, G.; Magliulo, G.; Petrone, C.; Prota, A. Shake table tests for the seismic fragility evaluation of hospital rooms. *Earthq. Eng. Struct. Dyn.* **2015**, *44*, 23–40. [CrossRef]
49. Feng, M.Q.; Shinozuka, M.; Kim, H.K.; Kim, S.H. Statistical analysis of fragility curves. *J. Eng. Mech.* **2000**, *126*, 1224–1231.
50. Dimitrakopoulos, E.G.; Paraskeva, T.S. Dimensionless fragility curves for rocking response to near-fault excitations. *Earthq. Eng. Struct. Dyn.* **2015**, *44*, 2015–2033. [CrossRef]
51. Petrone, C.; Di Sarno, L.; Magliulo, G.; Cosenza, E. Numerical modelling and fragility assessment of typical freestanding building contents. *Bull. Earthq. Eng.* **2017**, *15*, 1609–1633. [CrossRef]
52. Sieber, M.; Vassiliou, M.F.; Anastasopoulos, I. Intensity measures, fragility analysis and dimensionality reduction of rocking under far-field ground motions. *Earthq. Eng. Struct. Dyn.* **2022**, *51*, 3639–3657. [CrossRef]
53. Liu, H.; Huang, Y.; Qu, Z. A discretely damped SDOF model for the rocking response of freestanding blocks. *Earthq. Eng. Eng. Vib.* **2022**, *21*, 729–740. [CrossRef]
54. Zhang, J.; Makris, N. Rocking response of freestanding blocks under cycloidal pulses. *J. Eng. Mech.* **2001**, *127*, 473–483.
55. Weir, G.; McGavin, P. The coefficient of restitution for the idealized impact of a spherical, nano-scale particle on a rigid plane. *Proc. R. Soc. A Math. Phys. Eng. Sci.* **2008**, *464*, 1295–1307. [CrossRef]
56. Čeh, N.; Jelenić, G.; Bićanić, N. Analysis of restitution in rocking of single rigid blocks. *Acta Mech.* **2018**, *229*, 4623–4642. [CrossRef]
57. Diamantopoulos, S.; Fragiadakis, M. Seismic response assessment of rocking systems using single degree-of-freedom oscillators. *Earthq. Eng. Struct. Dyn.* **2019**, *48*, 689–708. [CrossRef]
58. Makris, N.; Konstantinidis, D. The rocking spectrum and the limitations of practical design methodologies. *Earthq Eng Struct Dyn.* **2003**, *32*, 265–289. [CrossRef]
59. Vassiliou, M.F.; Mackie, K.R.; Stojadinović, B. Dynamic response analysis of solitary flexible rocking bodies: Modeling and behavior under pulse-like ground excitation. *Earthq. Eng. Struct. Dyn.* **2014**, *43*, 1463–1481. [CrossRef]
60. McKenna, F. OpenSees: A Framework for Earthquake Engineering Simulation. *Comput. Sci. Eng.* **2011**, *13*, 58–66. [CrossRef]
61. Nasi, K.T.J. Stability of Rocking Structures. Master's thesis, Purdue University, West Lafayette, IN, USA, 2011.
62. Klaboe, K.; Pujol, S.; Laughery, L. Stability of Rocking Structures. *Purdue Univ. Res. Repos.* **2017**. [CrossRef]

63. Klaboe, K.; Pujol, S.; Laughery, L. Seismic Response of Rocking Blocks. *Earthq. Spectra* **2018**, *34*, 1051–1063. [CrossRef]
64. Linde, S.A.; Konstantinidis, D.; Tait, M.J. Rocking response of unanchored building contents considering horizontal and vertical excitation. *J. Struct. Eng.* **2020**, *146*, 04020175. [CrossRef]